

NASA-CR-205093

Comparison of lidar backscatter with particle distribution and GOES-7 data in Hurricane Juliette

Maurice A. Jarzembki,¹ Vandana Srivastava,² Eugene W. McCaul, Jr.,² Gary J. Jedlovec,¹ Robert J. Atkinson,³ Rudolf F. Pueschel,⁴ and Dean R. Cutten⁵

Abstract. Measurements of calibrated backscatter, using two continuous wave Doppler lidars operating at wavelengths 9.1 and 10.6 μm were obtained along with cloud particle size distributions in Hurricane Juliette on 21 September 1995 at altitude ~ 11.7 km. Agreement between backscatter from the two lidars and with the cloud particle size distribution is excellent. Features in backscatter and particle number density compare well with concurrent GOES-7 infrared images.

Introduction

Lidars can be used to measure backscatter of atmospheric aerosols and clouds [Menzies and Tratt, 1994], where the backscatter magnitude is in part indicative of particle number density. Their high resolution capability provides a unique method of measuring fine-scale atmospheric variations [Srivastava *et al.*, 1995]. Recently, two National Aeronautics and Space Administration (NASA)/Marshall Space Flight Center (MSFC) continuous wave (CW) focused Doppler lidars obtained in-situ high resolution calibrated backscatter measurements in Hurricane Juliette as part of the 1995 NASA/Multicenter Airborne Coherent Atmospheric Wind Sensor (MACAWS) mission on board NASA's DC8 aircraft. Two traverses of Juliette's eye were made off the west coast of Mexico at altitude ~ 11.7 km on 21 September 1995. The two independent lidar data sets offered an opportunity for intercomparison and validation of the calibrated backscatter results. These were also intercompared with in-situ cloud particle size distributions obtained from NASA/Ames Research Center's forward scattering spectrometer probe (FSSP), the DC8 aircraft infrared (IR) surface temperature radiometer data, and the Geostationary Operational Environmental Satellites (GOES-7) 11 μm IR emission images with their corresponding estimates of cloud top temperature and height. At the time of the DC8 flight through Juliette, GOES-7 was in geosynchronous orbit over the equator and 135° W longitude and provided superior viewing geometry of the eastern Pacific ocean region. GOES-7 IR data for the 12-h period beginning at 1600 UTC and spanning the DC8 flight, were used to monitor the cloud development and structure of Juliette.

Meteorology, Flight, and GOES-7 Data

Juliette developed off the west coast of Mexico on 16 September 1995. It moved slowly west-northwestward and gradually intensified, reaching hurricane strength by 18

September. Juliette reached its maximum strength at 2100 UTC on 20 September, with peak winds of 64 m s⁻¹ (125 kt) and minimum central pressure of 925 hPa. At this time, eyewall decay-replacement cycles were occurring, with the old eyewall contracting and dissipating while a new, larger annular eyewall formed outside [Willoughby *et al.*, 1982]. Late stages of this cycle were observed at the time of the DC8 traversal of Juliette's core on 21 September. As the storm moved over cooler water it gradually lost strength, ultimately dissipating on 26 September.

During the DC8 flight around and through Juliette, the storm displayed a nearly symmetrical, rapidly expanding cirrus outflow shield, according to concurrent GOES-7 imagery. The storm's rainfall pattern, however, exhibited considerable azimuthal asymmetry, with heaviest precipitation located in the storm's core and in strong rainband convection along the storm's southern periphery, as diagnosed from the 85 GHz channel of the Special Sounder Microwave/Imager (SSM/I) at 1756 UTC on 21 September. Outer rainbands were absent on the storm's northern flanks, perhaps because of the presence of cooler ocean water and drier midtropospheric air. The small, old eyewall, still evident within the center of the new, larger annular eye, remained connected to the new eyewall by a vestigial spiral band structure in the storm's north quadrant, with a veil of thin cirrus covering the developing new large eye.

Flight through Juliette lasted ~ 2.5 -h, during which two traverses of the eye were made separated by ~ 1.6 -h. A GOES-7 IR image of Juliette at 2100 UTC (~ 21 min. after the first eye penetration) is shown in Fig.1. Flight track from 2010 to 2250

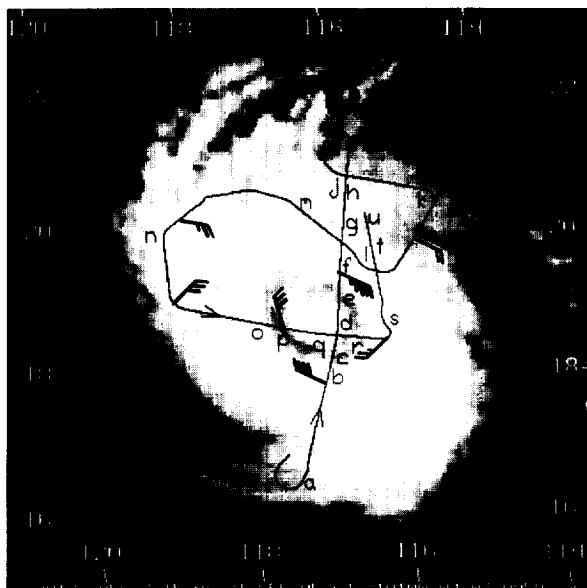


Figure 1. GOES-7 IR image of Hurricane Juliette on 21 September 1995 at 2100 UTC. The co-located position of the NASA DC8 flight track is shown from 2010 to 2250 UTC.

¹ NASA/Marshall Space Flight Center, Huntsville, AL

² Universities Space Research Association, Huntsville, AL

³ Lockheed Martin Corp., Huntsville, AL

⁴ NASA/Ames Research Center, Moffett Field, CA

⁵ University of Alabama in Huntsville, Huntsville, AL

Copyright 1997 by the American Geophysical Union.

Paper number 97GL00832.
0094-8534/97/97GL-00832\$05.00

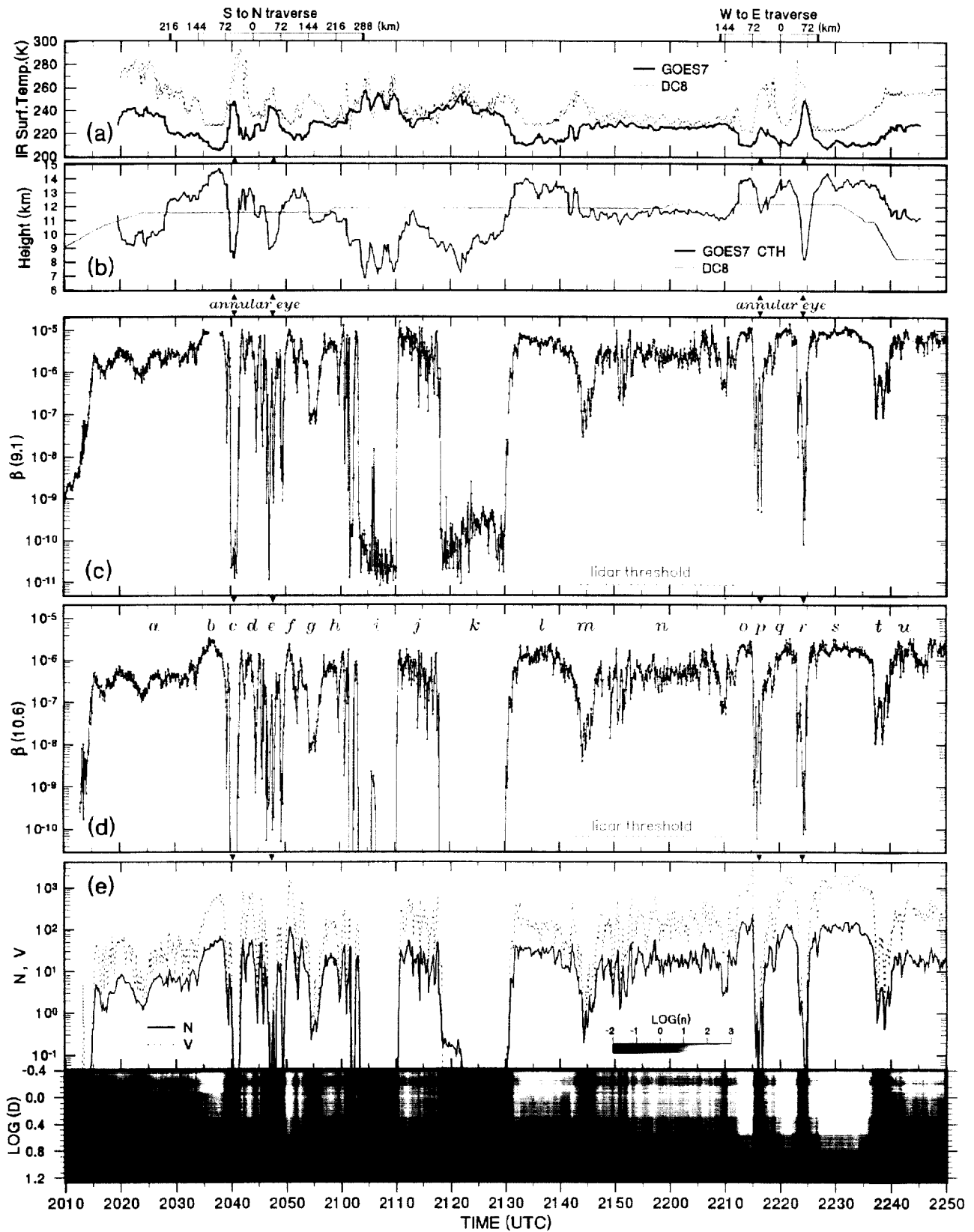


Figure 2. (a) Measured IR surface cloud-top temperature (CTT) from GOES-7 and DC8 radiometer and (b) calculated cloud-top height (CTH) from GOES-7 along the DC8 flight track. CW lidar backscatter β ($\text{m}^{-1} \text{sr}^{-1}$) measurements at (c) $9.1\ \mu\text{m}$ and (d) $10.6\ \mu\text{m}$ wavelengths; and (e) FSSP measurements of total particle number concentration N (cm^{-3}), inferred total particle volume V ($\mu\text{m}^3 \text{cm}^{-3}$), and shaded cross section of $\log(D)$. Broad-scale features labeled alphabetically on the $10.6\ \mu\text{m}$ β time series plot are identified in Fig. 1.

UTC is shown overlaid on the image with storm features labeled alphabetically along with wind vectors from the DC8 flight level data. From five GOES-7 IR images taken consecutively between 2030 and 2230 UTC, the digital IR cloud-top temperature (CTT) was determined at the co-located position of the DC8 flight track, and is shown in Fig.2(a). The IR temperature corresponding to the closest pixel to the flight track location was used to assign a CTT value. Data resolution is ~ 8 km which corresponds to a ~ 33 -s portion of DC8 data stream (DC8 speed ~ 240 m s⁻¹). Accuracy of CTT estimates is believed to be better than 0.5 K. Also, Fig.2(a) shows the IR temperature from nadir-viewing radiometer on DC8. This operates in the spectral band of 9.5 to 11.5 μm and has a 2° field of view which autoranges over three temperature spans to cover 208 to 328 K with ± 0.5 K accuracy.

CTT from GOES-7 was converted to cloud-top height (CTH), shown in Fig.2(b), using corresponding temperature and associated geopotential height from a reference climatological thermodynamic profile stratified by season and latitude. This conversion is good when clouds are opaque with large optical depth, while thin clouds with a low thermal emissivity can give erroneously low CTH values. The DC8 flight altitude is also shown in Fig.2(b). There are seven distinct, broad-scale regions where the CTH is greater than the DC8 cruising altitude.

Data shown in Figs.2(a, b) allow intercomparison of GOES-7 satellite and in-situ DC8 temperature measurements in several flight segments. Between 2057 to 2127 UTC and 2146 to 2210 UTC, where DC8 was above or near cloud top, the estimated CTT from GOES-7 agrees with DC8 radiometer. However, in regions like the annular eye, the location and width of the features agree well but the magnitude does not. This difference is a result of the different spatial resolution of the two radiometers. When DC8 was in dense cloud, GOES-7 detected a lower CTT associated with a CTH above DC8 flight altitude.

Lidar Backscatter and Particle Distribution

The CW Doppler lidars, operating at 9.1 and 10.6 μm CO₂ wavelengths, are coherent homodyne instruments measuring the backscattered signal from particles in the lidar sample volume. The lidar beams were focused at ~ 54 m from the aircraft, beyond the DC8 right wing. Details of the lidars and data acquisition are given elsewhere [Rothermel *et al.*, 1996]. Measured signal-to-noise ratio (SNR) was converted to absolute backscatter coefficient β (m⁻¹ sr⁻¹) based on an aerosol calibration technique [Jarzembski *et al.*, 1996]. Both lidar measurements of β were obtained with 3-s integration times, giving horizontal along-track resolution of ~ 0.72 km and corresponding integrated sample volume of ~ 400 m³ for DC8 ground speed of ~ 240 m s⁻¹. Absolute uncertainty in the β measurements is $\sim 20\%$, while relative uncertainty between adjacent β values is less than 1%, due mostly to subtle laser power fluctuations. The measured sensitivities of the 9.1 and 10.6 μm lidars were $\sim 8 \times 10^{-12}$ m⁻¹ sr⁻¹ and $\sim 5 \times 10^{-11}$ m⁻¹ sr⁻¹, respectively.

Using these two airborne CW lidars, absolute calibrated β was obtained for the first time in the upper levels of a hurricane. β at 9.1 and 10.6 μm are shown in Fig.2(c) and (d), respectively. Dramatic β variations, some spanning over five orders of magnitude, are evident, showing a variety of features at 20-150 km scales. These features are labeled alphabetically on the 10.6 μm β time series plot in order to facilitate comparison with the GOES-7 data [Figs.1 and 2(b)]. Very fine-scale (~ 2 km scale) β variations were also detected. Both independent β measurements exhibit similar features that agree spatially, temporally, and in relative magnitude. The correlation coefficient between β for the two lidars is ~ 0.94 .

The total particle number density, N , and the particle size distributions, $dn/d\log(D)$ (where n is the number of particles in the size bin around size D) at 10-s integration time from the FSSP (sample volume $\sim 10^{-3}$ m³) are shown in Fig.2(e). A detailed description of the FSSP is given in Cutten *et al.*, 1996. Total particle volume V obtained from a spherical particle approximation is also shown in Fig.2(e) to give a rough estimate of cloud ice content. At diameter ~ 1 μm , specular reflection off ice particle surfaces could cause the enhanced particle count artifact. Although caution needs to be exercised in interpreting FSSP size distribution data taken inside clouds in the presence of ice particles [Gardiner and Hallett, 1985], the agreement between the two independent data sets, β and N , (along with $dn/d\log(D)$ and V) is excellent with logarithmic correlation of ~ 0.86 , depicting the direct proportionality between β and N .

Hurricane Eye Traverses

The DC8 entered the north periphery of Juliette at ~ 1900 UTC at altitude ~ 3.1 km. After skirting the storm's western edge, it began a slow ascent along the storm's south flank at 1954 UTC. By 2024 UTC it reached a cruising altitude of ~ 11.7 km, and positioned itself for the first eye traverse from south to north. At the time, the original eye was weakening as its eyewall cloud collapsed within a new, larger eye, giving the appearance of an annular eye with clouds in the central region.

Located within the hurricane's outer cirrus cloud anvil (region *a*), dense cirrus decks were encountered at ~ 2018 and ~ 2027 UTC with enhanced β and N . The magnitude of the fine-scale β variations in (*a*) were smaller than in the rest of the traverses. At ~ 2034 UTC, a very dense eyewall cloud (*b*) was encountered, with a sharp increase in β and N . The strength of β was so extreme that the 9.1 μm lidar became temporarily saturated. In this eyewall cloud, there was intense precipitation which lasted for several minutes. Here, the sun was completely obscured in the zenith-looking video record because of dense clouds and precipitation. During this time, the CTT decreased dramatically, showing that the eyewall CTH was ~ 3 km above the DC8, which was the highest CTH encountered.

An extremely low- β remnant of clean atmosphere (*c*) from the new annular eye, with a drop in β of almost 6 orders of magnitude, was encountered immediately after passing through (*b*). GOES-7 and DC8 radiometer IR temperatures rose dramatically here, indicating a CTH lower than flight level. The traverse of this region lasted ~ 80 -s corresponding to a distance of ~ 20 km. β in (*c*) is similar to typical aerosol β seen on the return flight along the southern California coast at ~ 12.8 km altitude and in clean air in remote regions over the Pacific ocean in the upper troposphere [Srivastava *et al.*, 1996] at ~ 8 km altitude.

Cirrus from the old eyewall cloud (*d*) was detected inside the new annular eye, causing a dramatic increase in β and N as well as a decrease in CTT and increase in CTH. In (*e*), there was strongly varying β from clouds linking the new and old eyewalls across the north part of the annular eye. In (*f*), additional cirrus having high β and N was seen north of the annular eye with a drop in CTT and rise in CTH. Although the sun was again obscured in (*f*), no precipitation was observed. Region (*h*) consisted of cirrus cloud bands outside the immediate eyewall cloud, between thin cirrus (*g*) having low β and N and clearer air (*i*) with extremely low β and N .

As the DC8 turned within (*i*), it re-entered the same cloud band (*h*), now labeled (*j*). This traverse from (*i*) to (*j*) showed an abrupt increase in β and N , as dramatic as the change from (*b*) to (*c*). Levels of β and N gradually decreased eastward along this trailing cloud band, before dropping abruptly again in (*k*). In (*i*)

and (*k*), the CTT rose, indicating lower CTH with cloud-free air aloft at the DC8 cruising altitude. The DC8 then flew along the north eyewall cloud (*l*). β and N gradually decreased in (*m*), a band of clearer air similar to (*g*). The cirrus cloud band (*n*) outside the most intense part of the hurricane displayed considerable β variations. This is probably because DC8 flight level was very near the CTH, so that the lidars sampled anvil-top waves having large particle density fluctuations, also seen as fluctuations in particle size in $n(D)$ (Fig.2e).

At ~2209 UTC, the west-to-east traverse of the eye began. β and N decreased briefly at ~2210 UTC and then rose in the western eyewall cloud (*o*). At ~2214 UTC, there was a further increase in β due to heavy precipitation that lasted ~1 min. β and N then dropped dramatically in the clearer air of the new eye (*p*). In (*q*), there was a large increase in β and N, in association with rainband clouds merging in the original eye, stronger than that seen in (*d*) ~1.6-h earlier, while the clearer air (*r*) has a structure similar to (*p*). β and N were very large in the eastern eyewall cloud (*s*), but no heavy precipitation was observed there. In each of the eyewall regions sampled (*b*, *d*, *f*, *o*, *q*, *s*), largest n occurred in the large size regime. At 2231 UTC, DC8 began a slow descent and reached (*t*) with small β and N at ~11.0 km altitude. Regions (*g*), (*m*), and (*t*) are all in relatively clear air and show similar features in β and N. Finally, (*u*) is a cloud band outside the immediate eyewall cloud as encountered earlier in (*h* and *j*); this time the feature was sampled at ~8.2 km altitude. Here, β is comparable to (*o*, *q*, *s*), but N has dropped considerably relative to β , which may be due to possible changes in particle morphology at the lower altitude and higher temperature.

Discussion

This is the first time a comparison has been made among satellite imagery parameters and in-situ calibrated β from airborne CW lidars and cloud particle size distributions in a hurricane. Both the 9.1 and 10.6 μ m lidars tracked the changing features in Juliette despite the dramatic variability in β magnitude. Nearly every variation in β is reflected in N, $dn/d\log(D)$, and V and in the more coarse CTH, in spite of the significant differences in the sample volumes of the in-situ and satellite instruments. The size distributions provide an excellent data set for modeling scattering from cloud ice particles, with validation provided by the concurrent calibrated β measurements. β at 9.1 and 10.6 μ m differ by the wavelength dependence factor. Lidar β ratio between 9.1 and 10.6 μ m is measured to be around -6 ± 2 . Assuming a log-normal size distribution for cloud particles under a spherical approximation with equivalent sphere radii (mean radius of several microns), Mie theory gives β ratios ranging from 3 to 7. A lower ratio of ~2 would indicate presence of sulfuric acid aerosols [Srivastava *et al.*, 1995]; however, this was not encountered even under the lowest β conditions within Juliette, suggesting little likelihood of stratospheric air intrusion, which would contain mostly sulfuric acid aerosols. This corroborates findings by Newell *et al.* (1996).

Within a cloud, the β variations give direct indications of cloud N variations, as shown by the excellent agreement between β and N. In a mature storm like Juliette, high β is associated with high N which indicates strong convective activity, leading to high CTH. Low β due to low N indicates lesser convective

activity which would not support a high CTH. Hence, whenever the DC8 is in clouds, variations of lidar-measured β along the flight track correspond to the crossing of contours of N in the field of cloud particle density (as seen in Fig.2e), the latter of which is in turn associated with the cloud activity as indicated by the CTH (Fig.2b). In regions where the CTH is above the DC8, comparison of CTH with the two separate in-situ data sets shows the correlation between $\log N$ and CTH, and between $\log \beta$ and CTH (remapped to a common grid of CTH data) to be ~0.6 and ~0.5, respectively. Because these correlations cannot fully account for differences associated with the dissimilar spatial resolutions of the in-situ versus satellite data sources, we suspect that the real correlation is even higher. Therefore, in vigorous convective systems CTH itself may be a possible indirect indicator of changes in the particle density field and β variations at a given height within the upper levels of the cloud. This suggests an intriguing possibility of using large-scale satellite data to infer some of the deep cirrus cloud microphysical parameters. However, more research should be pursued to verify this further and determine the detailed height dependence of the β -CTH and N-CTH correlations for various cloud types as well as their possible utility for parameterization of global backscatter fields within clouds.

Acknowledgments. Authors are grateful to R. Kakar, Office of Mission to Planet Earth, NASA Headquarters, for funding the NASA/MSFC CW lidars and NASA/ARC FSSP on the MACAWS mission and to D. Chambers and J. Rothermel for mission support. This work was partially supported under NASA contracts 95-193 and NAS8-39206.

References

- Cutten, D. R., R. F. Pueschel, D. A. Bowdle, V. Srivastava, A. D. Clarke, J. Rothermel, J. D. Spinhirne, and R. T. Menzies, Multiwavelength comparison of modeled and measured remote tropospheric aerosol backscatter over Pacific, *J. Geophys. Res.*, **101**, 9375-9389, 1996.
- Gardiner, B. A., and J. Hallett, Degradation of in-cloud forward scattering spectrometer probe measurements in the presence of ice particles, *J. Atmos. Oceanic Technol.*, **2**, 171-180, 1985.
- Jarzembski, M. A., V. Srivastava, and D. M. Chambers, Lidar calibration technique using laboratory-generated aerosols, *Appl. Opt.*, **35**, 2096-2108, 1996.
- Menzies, R. T. and D. M. Tratt, Airborne CO₂ coherent lidar for measurements of atmospheric aerosol and cloud backscatter, *Appl. Opt.*, **33**, 5698-5711, 1994.
- Newell, R. E., *et al.*, Atmospheric sampling of Supertyphoon Mireille with NASA DC-8 aircraft on September 27, 1991, during PEM-West A, *J. Geophys. Res.*, **101**, 1853-1871, 1996.
- Rothermel, J., D. M. Chambers, M. A. Jarzembski, V. Srivastava, D. A. Bowdle, and W. D. Jones, Signal processing and calibration of continuous-wave focused CO₂ Doppler lidars for atmospheric backscatter measurement, *Appl. Opt.*, **35**, 2083-2095, 1996.
- Srivastava, V., D. A. Bowdle, M. A. Jarzembski, J. Rothermel, D. M. Chambers, and D. R. Cutten, High resolution remote sensing of sulfate aerosols from CO₂ lidar backscatter, *Geophys. Res. Lett.*, **22**, 2373-2376, 1995.
- Willoughby, H. E., J. A. Clos, and M. G. Shoreibah, Concentric eye walls, secondary wind maxima, and the evolution of the hurricane, *J. Atmos. Sci.*, **39**, 395-411, 1982.

(Received November 7, 1996; revised February 27, 1997, accepted March 10, 1997)